Nanopatterning of Transition Metal Surfaces *via* Electrochemical Dimple Array Formation

Sherdeep Singh, Warren R. T. Barden, and Peter Kruse*

Department of Chemistry, McMaster University, 1280 Main Street West, Hamilton, Ontario, L8S 4M1, Canada

ABSTRACT Nanoscale surface patterning is of great importance for applications ranging from catalysts to biomaterials. We show the formation of ordered nanoscale dimple arrays on titanium, tungsten, and zirconium during electropolishing, demonstrating versatility of a process previously only reported for tantalum. This is a rare example of an electrochemical pattern formation process that can be translated to other materials. The dimpled surfaces have been characterized with scanning electron microscopy, transmission electron microscopy, atomic force microscopy, and X-ray photoelectron spectroscopy, and electrochemical conditions were optimized for each material. While conditions for titanium and tungsten resemble those for tantalum, zirconium requires a different type of electrolyte. Given the appropriate electropolishing chemistry, formation of these patterns should be possible on any metal surface. The process is very robust on homogeneous surfaces, but sensitive to inhomogeneities in chemical composition, such as in the case of differentially etched alloys. An alternative process for some materials such as platinum is the coating of a dimpled substrate with a thin film of the required material.

KEYWORDS: nanoscale pattern formation · electropolishing · surface structure · self-assembly

The preparation of surfaces with uniform nanoscale patterns is a challenge that has been addressed in a variety of ways,[1−7] because their applications are wide-ranging, from electronic (*e.g.*, memory devices) and electrophotonic (*e.g.*, solid state lighting and solar cells) materials over catalysts to biocompatible surfaces. The quest continues, because each patterning method comes with its own set of challenges and limitations. Optical lithography, for example, has hit its resolution limits; electron beam, ion beam, or scanning probe lithographies are slow; imprint lithography, just as the previously mentioned methods, requires expensive equipment and is then still limited to reasonably flat surfaces. Self-organization strategies have been explored as alternatives, in many cases relying on the formation of an ordered mask which is then used to imprint structure onto the substrate.[6,7] The reason for this approach is that self-organizing systems tend to be very material specific, which is why for each proposed strategy a particular mask material is chosen on the basis of its ability to be driven into an ordered state. Direct processes for surface pattern formation are harder to come by, but examples exist.

Porous anodic oxide formation and electropolishing are two electrochemical approaches to surface patterning.[8] Anodic oxidation involves oxidation of the anode surface in an electrolyte that is unable to attack (dissolve) the formed oxide. If the electrolyte is able to dissolve only the electrode material or a thin oxide film in the presence of a strong electric field, while a thicker oxide film is rendered inert, a porous anodic oxide may be formed. If the oxide is dissolved rapidly, while the unoxidized electrode material is either inert or only dissolved at a much lower rate, the anode surface will be electropolished, with no anodic oxide remaining. So far, only porous anodic oxide formation has been explored in more detail for a variety of materials, including aluminum,[9−11] titanium,[12] tantalum,[13,14] and niobium.[15] In the case of aluminum, ordering of the pores can grow during the anodization process, which has been exploited in a 2-step process.[16] Pores in these oxides are always disordered, unless the surface is prepatterned prior to oxide formation.[10,11,14]

In the case of aluminum, prepatterning is possible not only by imprinting or lithography but also with the help of a number of ordered nanostructures that have been reported to arise during electropolishing of aluminum surfaces.[17−21] The origins of these patterns have been studied and mechanisms have been proposed,[22−25] but nobody has ever succeeded in translating them to other surfaces. Striped, spiral, or dotted patterns of various length scales have also been observed during

*Address correspondence to pkruse@mcmaster.ca.

Received for review June 16, 2008 and accepted November 11, 2008.

Published online November 21, 2008. 10.1021/nn8003789 CCC: $40.75

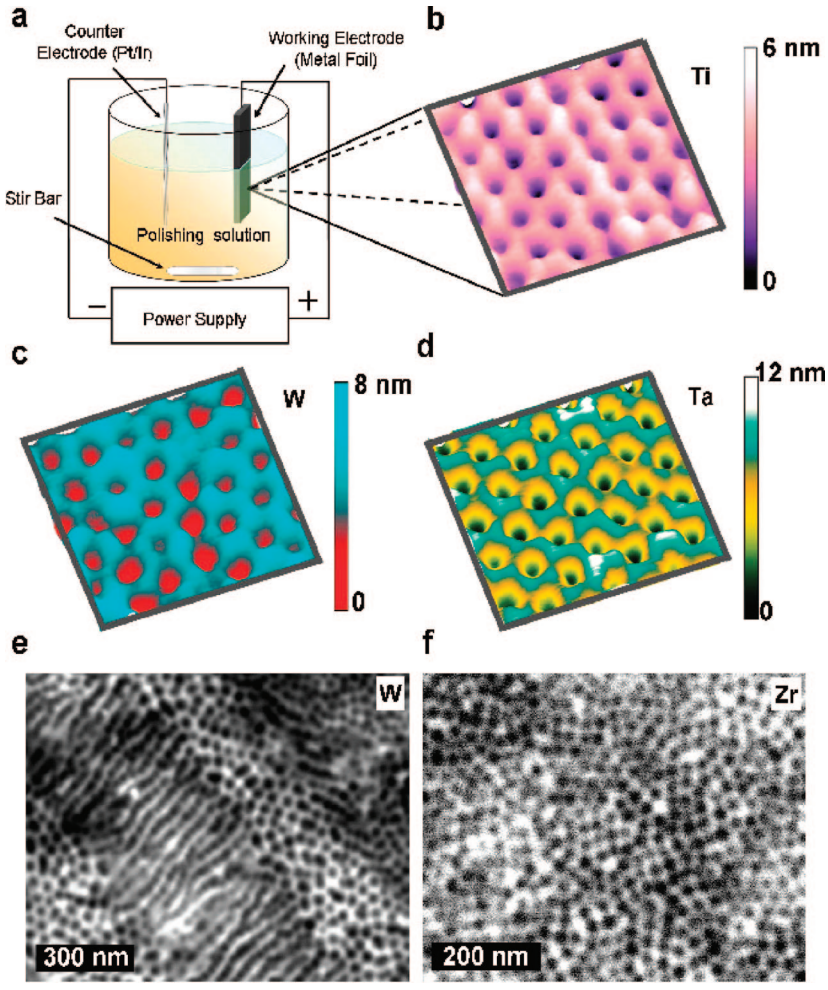

Figure 1. Formation of hexagonal and striped patterns on titanium, tantalum, tungsten and zirconium surfaces. (a) Illustration of electrochemical setup. Tapping-mode topographic (3D) AFM image of (b) titanium after electropolishing in 8:2 H_2SO_4/HF solution for 2 min at 15 V, (c) tungsten after electropolishing in 93:7 H_2SO_4/HF solution for 5 min at 15 V, (d) tantalum after electropolishing in 9:1 H_2SO_4/HF solution for 5 min at 15 V. Image dimensions for panels b−d are 300 × 300 nm^2. (e) SEM image of hexagonal and striped patterns on the tungsten surface. (f) SEM image of hexagonal patterns on the zirconium surface after electropolishing in 0.5 M NH_4F solution for 5 min at 20 V.

electropolishing or electroplating of titanium,[8] Zr_3Al alloy,[26] a silver antimony alloy,[27] copper,[28] and tantalum.[29,30] In particular, electropolishing of tantalum surfaces has been reported to result in highly ordered surface structures,[29−33] which were recently revealed to be arrays of shallow dimples.[32]

Here we show that the previously reported formation of ordered arrays of dimples on tantalum at the nanoscale is also applicable to titanium, tungsten, and zirconium and postulate that, given an appropriate electropolishing chemistry, these patterns can be formed on virtually any metal or semiconductor surface. While pattern formation during electropolishing has been observed before, this is the first time that such a process has been extended beyond the material on which it was originally observed. Scanning electron microscopy (SEM), transmission electron microscopy (TEM), atomic force microscopy (AFM), and X-ray photoelectron spectroscopy (XPS) were used to confirm the metallic nature of the ordered dimple structure.

DISCUSSION AND RESULTS

Dimple Morphologies from Electropolishing. Using a simple two-electrode electrochemical polishing cell (Figure 1a), ordered arrays of dimples can be generated reproducibly on titanium (Figure 1b), tungsten (Figure 1c,e), tantalum (Figure 1d), and zirconium (Figure 1f). AFM measurements indicate that tantalum dimples are on average 8−10 nm deep (Figure 1d), tungsten dimples are 5−6 nm deep (Figure 1c) and titanium dimples are 2.5−4 nm deep (Figure 1b). The ordered dimple patters were uniform across the entire surface for titanium, whereas for tungsten impurities played a role and under certain circumstances stripes were also observed (Figure 1e). Zirconium is the exception in this study in that a very different electrolyte had to be used, with the result of somewhat smaller dimples (40 nm compared to 55 nm in the cases of Ta, Ti, and W) and some oxidized areas remaining at the surface. The details of each system are described later.

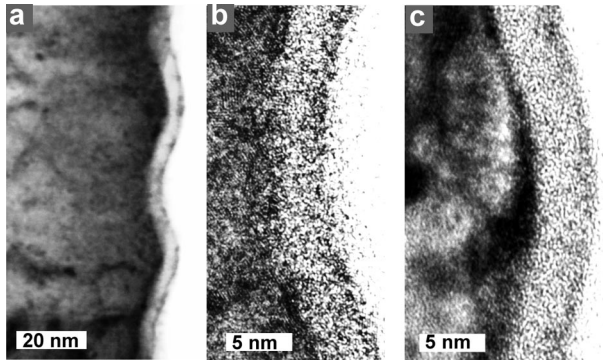

Figure 2. The dimple pattern is of metallic nature, as determined by cross-sectional TEM for tantalum and high resolution core-level spectra for titanium and tungsten before and after dimpling: (a) cross-sectional TEM image of dimples on tantalum; (b) zoom-in onto bottom part of dimple; (c) zoom-in onto crest area.

We have previously shown that on average the dimpled tantalum surface is covered by an oxide film of comparable thickness to a native oxide.[32] However, it was not clear whether the oxide thickness varies between the bottom of the dimples and the top of the ridges, as it would be expected if any substantial amount of oxide film was present during the electropolishing process, and possibly at the root of the pattern formation. We have now been able to perform transmission electron microscopy (TEM) on a tantalum sample (Figure 2) that was cross-sectioned using a fo-

cused ion beam (FIB). The depth of the dimples is identical to what was found by AFM (about 8 nm).[30] The oxide film is shown to be amorphous and very uniform in thickness (about 4 nm) and morphology in all locations, indicating that modulations in the oxide layer do not play any role in the pattern formation process, as it would have been expected if the dimple formation process would have be analogous to porous oxide formation.[9,23,25]

If we go outside a narrow window of electrolyte composition and applied potential, the reaction (oxidation, dissolution) speeds change sufficiently to either cease pattern formation due to slow-down or become turbulent and less regular (Figure 3). There is indeed a certain window in electrolyte composition available for dimple formation. The 9:1 ratio in the electrolyte composition was optimized for best electropolishing performance a long time ago, taking into account micrometer-scale surface roughness as well.[28] While ratios of 6:4 (Figure 3a), 8:2 (Figure 3b), and 8.5:1.5 (Figure 3c) still achieve nanoscale structuring, the resulting structures are less and less regular and ordered as the composition departs from the optimum value. The impact of anode potential has been discussed by us before.[32,33] The dimple size is dependent on the applied potential, with smaller potentials resulting in smaller dimples. This indicates that the dimple density is not coupled to surface defect density as it has been suggested for aluminum.[19] A potential below 10 V will still lead to electropolishing, but the order deteriorates rapidly. Too high of a voltage on the other hand causes an increase in the speed of anodic oxide formation beyond the maximum speed of dissolution, leading to the formation of a disordered porous oxide (Figure 3d). Both effects can be understood when taking into consideration the need for balance between the speeds of oxide formation, oxide dissolution, and transport of reactants and products to and from the electrode in order to achieve electropolishing.

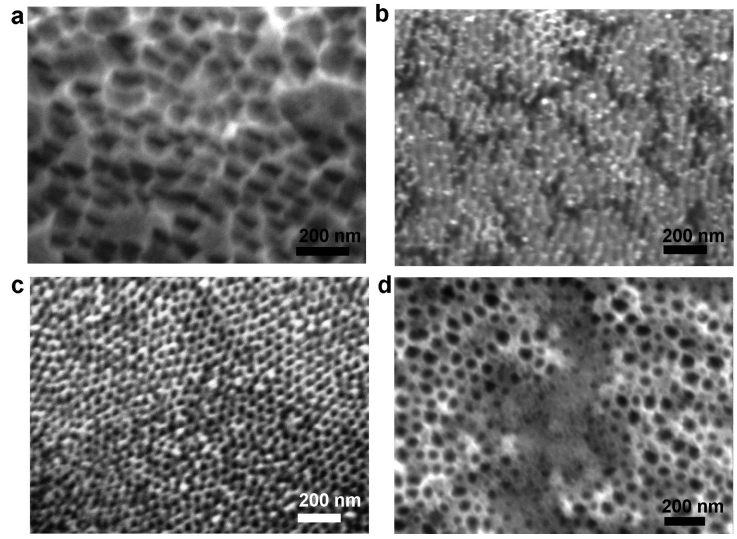

Figure 3. SEM images of electropolished tantalum showing the deterioration of the long-range order of dimples as one moves away from the narrow electrochemical regime of ordered pattern (dimples) formation by changing the concentration or applied voltage: (a) 6:4 H_2SO_4/HF, 15 V, 30 s; (b) 8:2 H_2SO_4/HF, 15 V, 5 min; (c) 85:15 H_2SO_4/HF, 15 V, 5 min; (d) 9:1 H_2SO_4/HF, 25 V, 2 min.

Titanium. Figure 4 shows a large area SEM image of a dimpled titanium surface, demonstrating the reproducibility of the process over large surface areas. It can be seen that grain boundaries and residual surface roughness do not impact the dimple pattern. In fact, this image is representative of a large number of images taken by us on several samples. Both tantalum[32] and titanium show ordered dimple patterns with excellent reproducibility (see also Supporting Information).

XPS proves that the dimpled titanium surfaces are also metallic, with only a native oxide cover (Figure 5b,d), when compared to unpolished surfaces (Figure 5a,c). Survey spectra of polished samples show slight incorporation of fluorine and sulfur into the dimpled samples (see Supporting Information). This is expected, because metal oxides grown in concentrated acids are known to incorporate electrolyte anions (F^- and SO_4^{2-}) in the whole depth of the native oxide film and even in the metal part adjacent to the metal/oxide interface. In addition to characteristic SEM images of the untreated and dimpled surfaces, Figure 5 also shows deconvoluted Ti 2p peaks of both surfaces. In both cases, the titanium signal from titanium oxide dominates the peak. Together with suboxides, over 90% of the signal comes from titanium in the superficial oxide film. Since the inelastic mean free path of the photoelectrons amounts to several nanometers in most solids, however, the metallic titanium signal from the bulk metal can be picked up. The untreated surface is essentially covered by a passive native oxide with a self-limiting thickness upon prolonged exposure to air. The ratio of oxide to metal signal decreases slightly for the dimpled surface, indicating that the dimple structure is metallic in nature, with only a minimal oxide cover as it is to be expected after exposure to air.

As in the case of tantalum, dimpling occurs on titanium inside a fairly narrow electrochemical window. As opposed to tantalum, this kind of electrolyte mixture has not previously been recommended as an electropolishing solution for titanium. Given a certain simi-

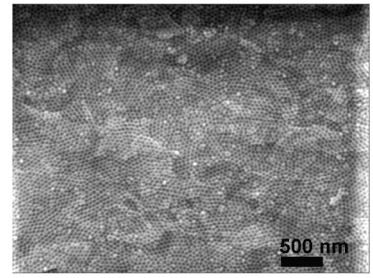

Figure 4. Characteristic SEM micrograph of a larger area of a Ti surface after dimpling (electropolishing).

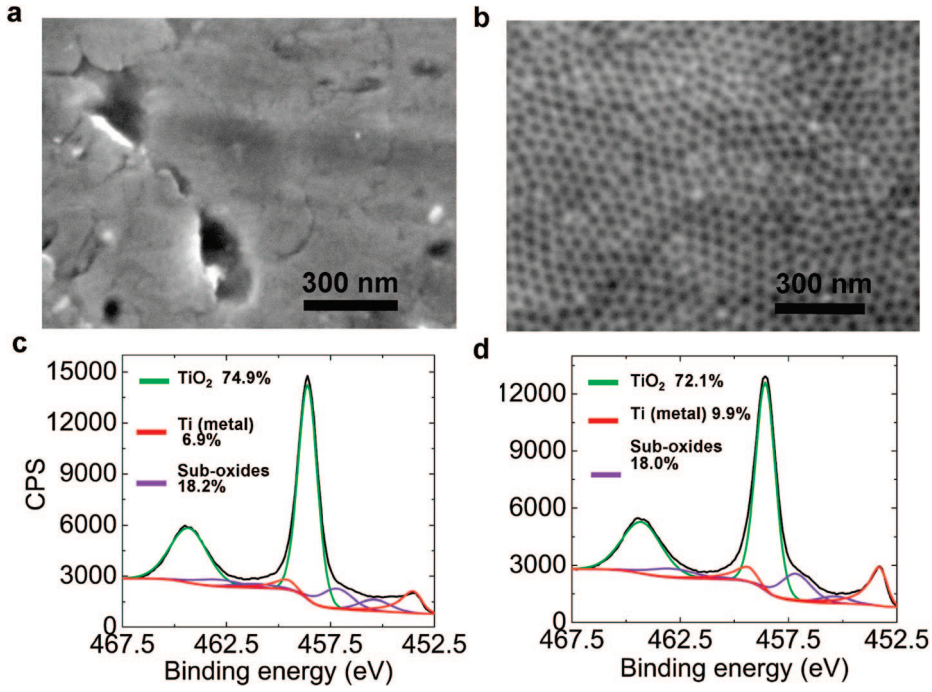

Figure 5. Comparison of SEM images and XPS spectra of titanium foil before and after dimpling: (a) SEM image of the untreated titanium surface; (b) SEM image of the dimpled titanium surface; (c) deconvoluted Ti 2p peak of the untreated titanium surface; (d) deconvoluted Ti 2p peak of the dimpled titanium surface.

larity between the chemistries of the transition metals in that particular corner of the periodic table, however, it is not entirely surprising that suitable conditions can be found, as long as the different electrode processes (oxidation, dissolution, transport) are in balance. Notably, the optimal potential (and, to some extent, the potential window) is the same for both metals, whereas the composition of the electrolyte differs slightly to account for the differences in chemistry. The potential not only determines the speed of oxide formation, but also impacts the electrochemical system in other ways, for example, by modulating the thickness of the electrochemical double layer and attracting or repulsing ionic reactants with varying rigor.

Tungsten. The dimple structures on tungsten are of similar periodicity and regularity. XPS once again shows that they are also clearly metallic in nature. Figure 7 shows SEM and XPS data comparing the untreated to the dimpled surface. In this case in fact, since electropolishing leads to a smoother surface, the corresponding spectrum of the dimpled surface (W 4f peak, Figure 7d) shows less oxide than the spectrum of the untreated surface (W 4f peak, Figure 7c). Survey spectra of the tungsten foil samples also show the presence of nickel on the surface (see Supporting Information).

Once again, ordered dimples are only observed at the surface under certain electrochemical conditions. The composition of the electrolyte had to be slightly varied, whereas the voltage window was comparable to tantalum and titanium. (Figure 8) At this point, without a detailed mathematical model of the electrode processes, the optimization of the dimple formation conditions is still a question of trial and error. It appears that the best conditions for dimple formation are given toward the upper end of the electropolishing potential, just before porous oxide formation sets in. On the other hand, we have found that the electrolyte composition had to be adjusted to bring this potential within the range of 15−20 V. If oxide dissolution was too efficient, the surface would be electropolished but not

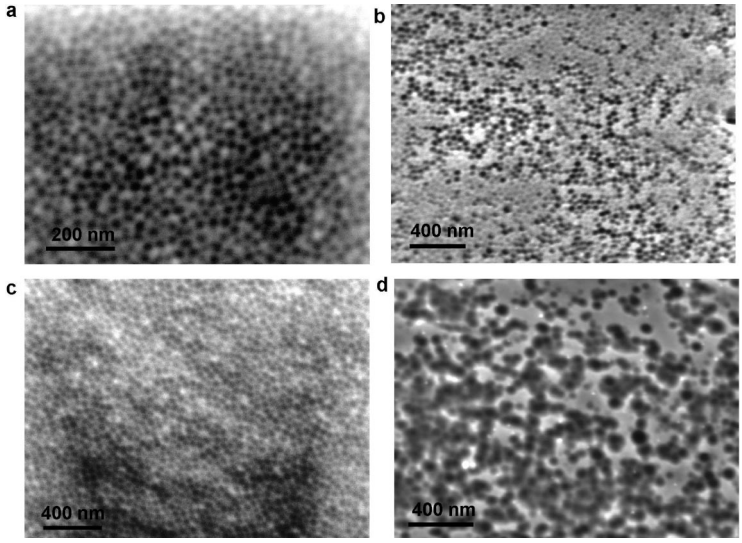

Figure 6. SEM images of electropolished titanium surface showing the deterioration of the long-range order of dimples as one moves away from the narrow electrochemical regime of ordered pattern (dimples) formation by changing the concentration or applied voltage: (a) 9:1 H_2SO_4/HF, 15 V, 1 min; (b) 7:3 H_2SO_4/HF, 15 V, 1 min; (c) 8:2 H_2SO_4/HF, 20 V, 1 min; (d) 8:2 H_2SO_4/HF, 6 V, 1 min.

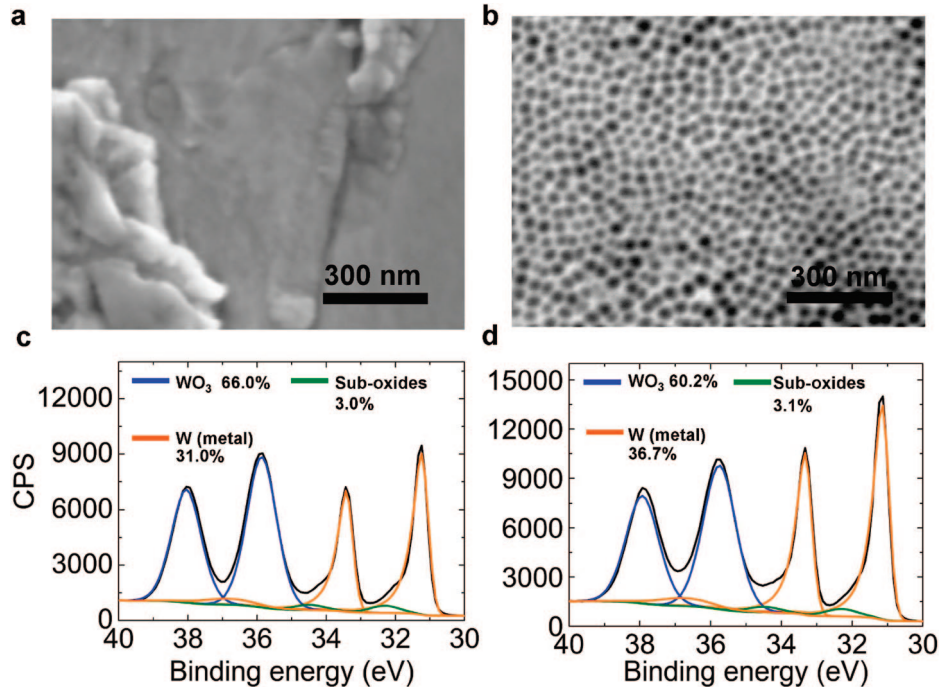

Figure 7. Comparison of SEM images and XPS spectra of tungsten ribbon before and after dimpling: (a) SEM image of the untreated tungsten surface; (b) SEM image of the dimpled tungsten surface; (c) deconvoluted W 4f peak of the untreated tungsten surface; (d) deconvoluted W 4f peak of the dimpled tungsten surface.

nanostructured, indicating that the dimpling regime may depend on diffusion limitation being achieved during a certain (optimal?) potential drop across the electrochemical double layer. Our proposed physical model of dimple formation is discussed in a later section of this paper. We are working toward developing mathematical models for this process, which would allow prediction of electropolishing conditions that would lead to dimpling on a wider variety of substrates.

It was observed in case of tungsten that the presence of trace amount of impurities gives rise to deterioration of order of dimples but not in case of tantalum and titanium. The certificates of analysis of Ti, Ta, and W showing the presence of different impurities are provided in the Supporting Information. To examine the spatial effect of other metal impurities on pattern formation on the W surface we mapped the elemental distribution using energy-dispersive X-ray spectroscopy (EDX) over part of the electropolished tungsten (99.95% pure) surface. A compositional SEM image of the metal surface is shown in Figure 9a and corresponding W, Ni, and O maps are displayed in color in Figure 9b−d. The darker regions in the SEM micrograph have higher concentration of Ni and O and exhibit either no dimples or poorly ordered dimples. High resolution XPS spectra of tungsten before and after dimpling (see Supporting Information) shows no noticeable peaks corresponding to Ni or NiO in the case of the untreated sample but clear peaks of Ni, NiO, and Ni_2O_3 in the case of the dimpled surface.

The combined analysis of EDX mapping and XPS data of unpolished and electropolished W surface leads to several conclusions. The electropolishing of a 99.95% pure tungsten surface leads to a substantial aggregation of nickel, which does not dissolve at the same speed as the tungsten. The nickel is instead left behind in the form of insoluble nickel oxide clusters. There was no evidence of iron and other metals present in the

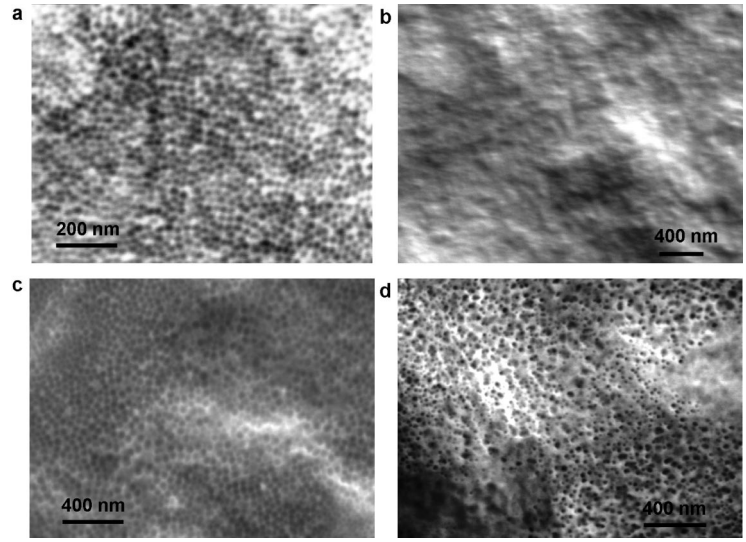

Figure 8. SEM images of electropolished tungsten surface showing the deterioration of the long-range order of dimples as one moves away from the narrow electrochemical regime of ordered pattern (dimples) formation by changing the concentration or applied voltage: (a) 93:7 H_2SO_4/HF, 10 V, 10 min; (b) 9:1 H_2SO_4/HF, 15 V, 10 min; (c) 95:5 H_2SO_4/HF, 15 V, 10 min; (d) 93:7 H_2SO_4/HF, 20 V, 10 min.

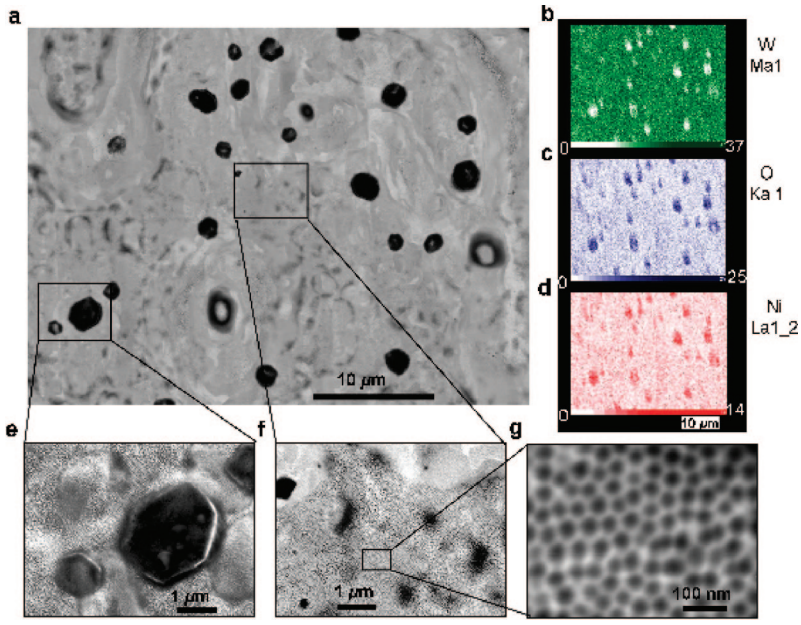

Figure 9. The presence of Ni as an impurity among other impurities in ppm amounts in W sample affects the order and quality of dimples. (a) SEM micrograph of electropolished W surface in compositional mode. (b) Elemental composition map of the same area as in (a) of W (c) O and (d) Ni obtained by EDX mapping. The intensity of the elements W, O, and Ni are shown on the map images itself with respect to the zero energy loss peak. (e) SEM micrograph in compositional mode showing the area having the NiO debris surrounded by irregular dimples. (f) SEM micrograph demonstrating that the regularity and order of dimples is high away from NiO rich areas. (g) Regular dimples in the area having no Ni present.

tungsten foil being left behind even as trace amounts on the surface showing that they dissolve or do not migrate to the surface. The oxygen concentration is higher in areas where there is more nickel and there are no dimples formed. Obtaining higher purity tungsten commercially proved to be nontrivial, so this may constitute an impediment to the practical application of the dimpling process on tungsten, unless high purity films can be deposited or a different electropolishing chemistry be utilized. On the other hand, the results also suggest that deliberate introduction of heterogeneities in the surface composition can be used to gain some form of control over the size and shape of the dimple arrays.

Zirconium. The electrolyte composition has to be varied in each case to achieve reaction speeds that ensure ordering. A mixture of concentrated HF (48%) and concentrated H_2SO_4 (95−98%) was used for titanium (20:80) and tungsten (7:93), comparable to the previously reported conditions for tantalum (10:90).[32] The concentrated sulfuric acid electrolyte leads to the formation of a lower quality oxide, which is necessary to speed up oxide dissolution.[34] Because zirconium is much more soluble in hydrofluoric acid than the other metals, a dilute aqueous ammonium fluoride solution (0.5 M NH_4F) was found to be more appropriate for it. F^- ions are still required to sustain the strong driving force required for ordered dimple formation, while bulk composition and viscosity of the electrolyte solution only play a minor role in the process. Whether fluorine ions are essential for the pattern formation or merely a part of the etching chemistry for selected metals may only be speculated at this point, although it should be noted that nanoscale patterns with a comparable appearance and length scale have previously been observed as a result of electropolishing of aluminum in a fluoride-free solution.[19] Figure 10a shows a partially dimpled zirconium surface. SEM images of dimpled zirconium reveal that the comparatively high speed of oxidation resulted in a mixture of dimpled regions (Figures 1f and 10b) and undissolved porous oxide (Figure 10c), making it difficult to determine the oxide layer thickness at the dimpled spots by XPS.

Dimple Evolution over Time. Time scale is an important indicator of how the dimples are formed. We therefore conducted time-resolved studies (Figure 11), clearly elucidating the time scale required for pattern formation. We started with an very flat, unpatterned, electropolished tantalum surface, obtained by peeling off an oxide film according to a previously published process (Figure 11a).[14] After only 500 ms we can observe the formation of dimples (Figure 11b). Since no dimples were observed after 300 ms, this marks about the time scale necessary for the electrochemical double layer to break up and order. The order of the dimples improves after a few seconds (Figure 11c) and stabilizes after about 1 min (Figure 11d). Since the electropolishing speed in our system is estimated to be around 20−50 nm/s,[32] the dimples are formed instantaneously at the onset of etching rather than as the result of an elaborate multistep process.

In addition to lateral ordering, it is also important to consider the depth evolution of the dimples. AFM imaging reveals that the depth of the dimples increases gradually at the same time as the order increases. (Figure 12) Neither AFM, TEM, nor SEM data taken by us indicate any temporal oscillation or instability in the dimple pattern once a steady state is reached within about a minute from the start of the electropolishing. This is much in contrast to most nonlinear electrochemical systems which often feature temporal oscillations.[35] Patterns originating from global coupling in an electrochemical system would result in a change of characteristic length scale with parameters of the outside system (electrode size and geometry of electrochemical cell, response time of potentiostat or power supply, *etc.*), whereas both Turing and electrohydrodynamic patterns have a smaller characteristic length scale that is invariant to external parameters.[35] Turing patterns can give rise to stationary spatially periodic structures,[36,37] but effectively require a permanent inhomogeneity in reaction speed. As our data demonstrates, the reaction speed is uniform across the entire

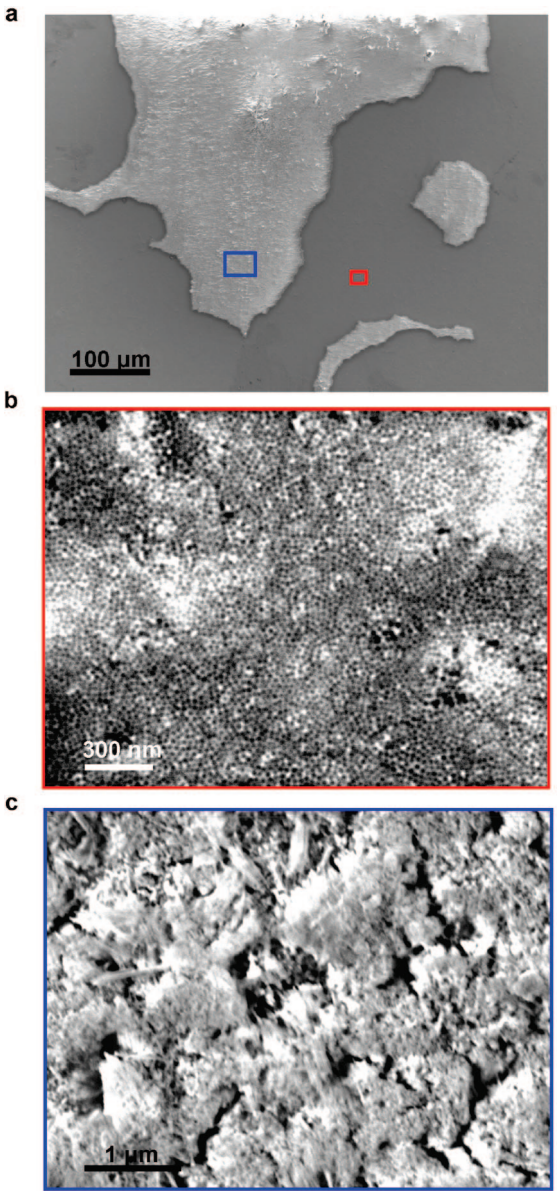

Figure 10. SEM images of the zirconium surface after electropolishing in 0.5 M NH_4F solution for 2 min at 20 V: (a) partially electropolished zirconium surface with parts having loose oxide on the surface; (b) electropolished area showing ordered dimples (close-up from area of panel a); (c) remnant irregular oxide present on the surface (close-up from area of panel a).

surface after an initiation period of about 1 min (Figures 2a and 12d) Initially, the etch speed at the bottom of the dimples is slightly faster than at the ridges. If we take the lower limit of our estimate for the global electropolishing speed at around 20 nm/s and consider the depth of the dimples after 5 s (Figure 12a,d) to be 4 nm, the ridges were etched about 100 nm deep during that time and the bottoms about 104 nm deep, a speed differential of 4%. The difference in etch speed is rapidly decreasing with time until it vanishes before 60 s are over.

A Model. We are now ready to decide the question of whether the pattern is determined by migration processes in the liquid or by surface topography or defects. Inherently, metal surfaces are prone to instabilities during electrodissolution, which may lead to random roughness on varying length scales.[38] Mechanisms proposed in the cases of porous silicon[39] or anodic porous oxides[9,23,25] are usually based on modulation of the field strength (and hence speed of oxide formation) by defects, oxide films, or other surface features. Positive feedback leads to enhanced etching at the same locations and causes pore formation. If these processes are stopped and resumed, the existing patterns are reinforced and amplified in the same location. The first indication that this is not the case in dimple formation comes from the uniform oxide thickness in the TEM cross-sectional view (Figure 2). It is also noticeable that grain boundaries have no impact on the order of the dimples (Figure 11d). Therefore the dimple formation is a very robust process that is not very sensitive to sample topography. Furthermore, while the size of the dimples remains fixed from the beginning (Figure 11b−d), the total number of dimples per unit area increases with the degree of ordering until a steady state is reached. This is characteristic of a dissipative process, but not of porous oxide formation. Final proof for this notion comes from a series of experiments where short DC pulses were applied to a fully formed dimple pattern on tantalum (Figure 13). In contrast to pore formation processes where pore formation is guided by field lines, the ion migration pattern in the double layer has to reform for each pulse. If a series of short pulses is applied, for example, 20 × 0.5 s or 10 × 1.0 s (Figure 13 panels a and b, respectively, separated by 0.5 s each), the pattern will form in a slightly different location for each pulse owing to a lack of boundary conditions, giving the dimples a somewhat gnawed appearance (Figure 13a,b). This shows that the double layer breaks up anew each time into a migration pattern, without memory of the previous location. The shallow dimples do not provide a strong enough template, as would be expected since not even steps along grain boundaries were able to template the growth. A longer pulse can erase the dimple pattern in the process (Figure 13c), whereas a sufficiently long pulse will lead to a reformed dimple pattern (Figure 13d).

We propose that nanoscale migration patterns can be induced using electromigration as a strong driving force leading to the breakup of an electrochemical double-layer. (Figure 14) At or near equilibrium, an elec-

TABLE 1. Comparison between Etching Conditions and Dimple Properties on Different Metal Surfaces

	Ta	Ti	W	Zr
dimple depth (nm)	10	3	6	n/a
periodicity of dimple pattern (nm)	55−60	55−60	55−60	40−45
optimal voltage (V)	15	15	15	20
etch mixture, H_2SO_4/HF	9:1	8:2	93:7	0.5 M NH_4F

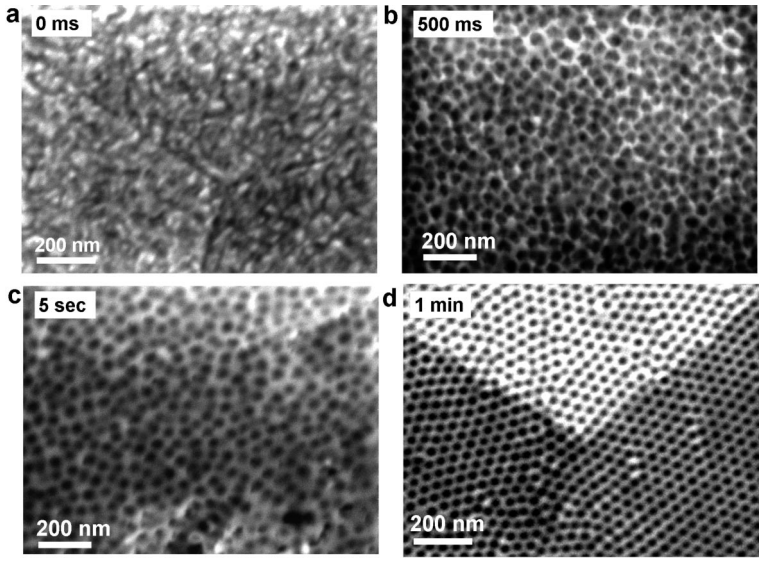

Figure 11. The dimple pattern appears within milliseconds, but takes several seconds to order. For all panels, a single rectangular DC pulse with 15 V ON voltage and 0 V OFF voltage was applied for different times: (a) electropolished, but unordered starting surface; (b) emerging dimple pattern after 0.5 s pulse; (c) increasing order after 5.0 s pulse; (d) well-ordered dimple pattern after 60.0 s pulse.

trochemical double layer forms at a metal electrode in contact with an electrolyte. (Figure 14a) Let us consider the example of a tantalum anode in an fluoride-containing electrolyte. As fluoride ions from the electrochemical double layer are consumed due to a reaction such as for example

$$Ta^{5+} + 7F^- \rightarrow TaF_7^{2-} \quad (1)$$

they are replaced by electromigration of F^- from the diffuse layer and then the bulk solution, displacing the reaction product in the process. The reactive F^- ions have a much higher charge to size ratio than the resulting TaF_7^{2-} complex and are therefore much more strongly attracted to the anode. This results in a lively exchange of species at the anode surface. At high reactions rates, the number of migrating ions becomes very large and they start to interact strongly, eventually leading to pattern formation as a means of facilitating migration (Figure 14b). If the system is driven too hard (e.g., at higher potentials), it becomes turbulent.[33] If the potential is removed, the electromigration stops and the patterns in solution disappear, leaving behind an etch pattern on the surface due to a slightly faster reaction rate at the bottom of the dimples where the fresh bulk solution hits the surface. Since the oxide is etched faster than the metal (a precondition for electropolishing as opposed to anodic oxide formation), however, the dissolution can keep up even at the ridges where the "used" solution leaves the surface, leading to shallow dimples at the surface rather than leading to the formation of pores. The chemistry has to be optimized individually for each surface because a balance needs to be achieved between the

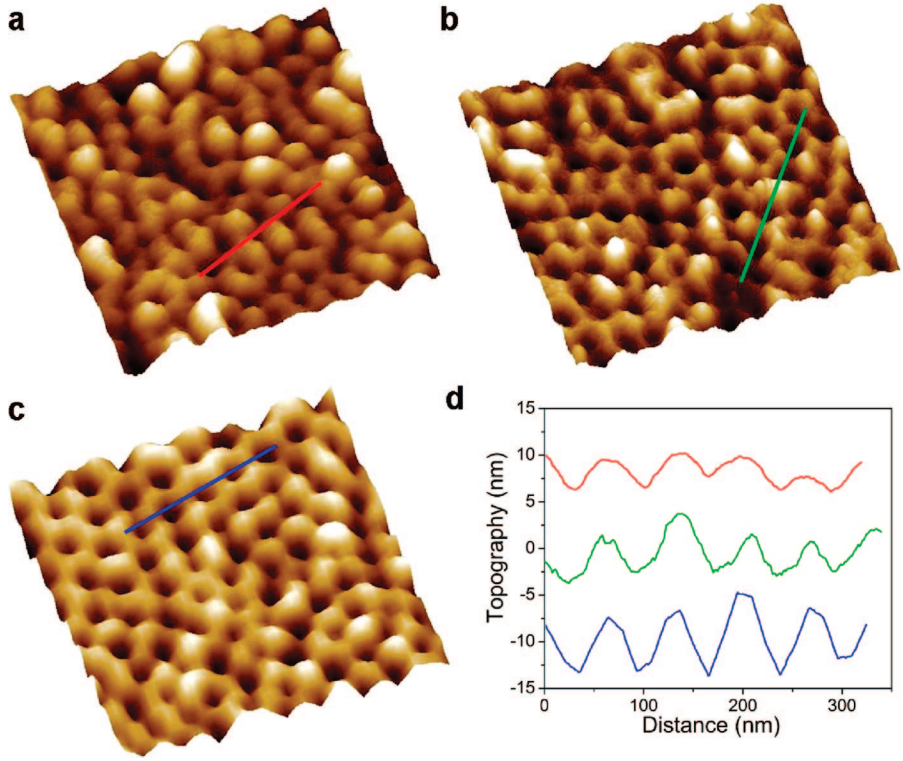

Figure 12. Atomic force microscopy images with 3D rendering shows the gradual increase in depth of the dimples with time on tantalum surfaces during electropolishing: (a) 5; (b) 30; (c) 60 s. (d) Height profiles of the dimples along the lines shown in panels a–c.

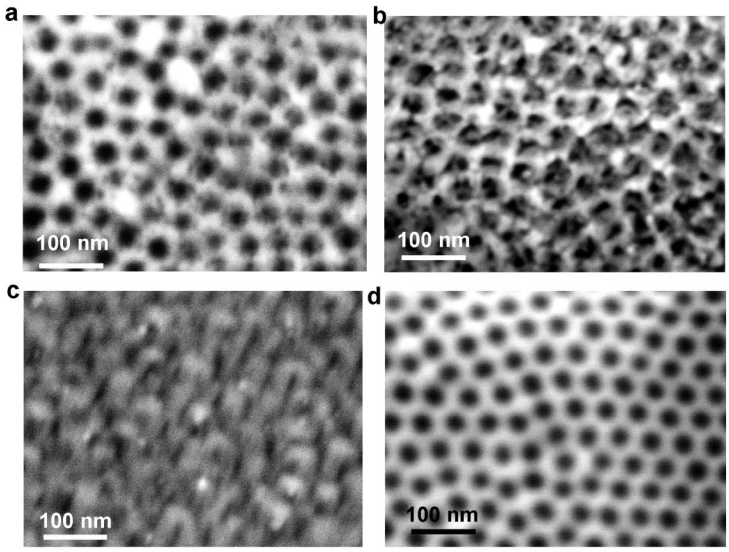

Figure 13. New patterns form each time the anodic potential is applied. For all panels, rectangular DC pulses with 15 V ON voltage and 0 V OFF voltage were applied for different times. (a) Pattern etched for 300 s ON, 30 s OFF; then 20 pulses, each 0.5 s ON, 0.5 s OFF. (b) Pattern etched for 300 s ON, 30 s OFF; then 10 pulses, each 1.0 s ON, 0.5 s OFF. (c) Pattern etched for 300 s ON, 30 s OFF; then 1 pulse for 10.0 s ON. This panel shows that the pattern can be erased. (d) Pattern etched for 300 s ON, 30 s OFF; then 1 pulse for 60.0 s ON. This shows that 60 s are enough to erase the previous pattern and then recreate a new pattern on the surface.

speeds of oxide formation (rate determining), oxide dissolution (very fast), and metal dissolution (very slow) in order for ordering to occur.

COMPARATIVE SUMMARY

A comparison between the different metals reveals many commonalities, but also some significant differences (Table 1). The optimal voltage stayed the same for all metals etched under an-aqueous conditions, so did the periodicity of the pattern. Larger voltages for these systems typically lead to slightly larger dimples (see refs 32 and 33 and Supporting Information). In the case of zirconium it was necessary to switch to a dilute aqueous ammonium fluoride solution. Here, the required optimum voltage was higher, but the resulting dimple size was smaller, clearly due to resulting changes at the electrolyte-anode interface, for example, properties of the electrochemical double layer. The regular pattern formation on metals etched under an-aqueous conditions was highly sensitive to the composition of the solution. In contrast to the constant periodicity of the dimple pattern for these systems, the depth of the dimples varied significantly between metals, but never came close to fulfilling the IUPAC definition of a pore (depth equal or greater than radius).

While we have demonstrated that electropolishing can be used to dimple a variety of metal surfaces, it will be a challenge to elucidate recipes for every single metal in the periodic table. However, thin metal films can be deposited onto the dimpled surfaces and annealed without damage to the dimple arrays or the substrate. The versatility of the dimple structures can therefore be greatly enhanced by coating thin films of the desired surface material onto dimpled substrates. To illustrate this process, we performed metalization and annealing experiments under controlled conditions (see methods section) using platinum (Figure 15a−c) and nickel (Figure 15d). Platinum does not dewet the surface even after annealing to 650 °C for 5 min and continues to form a smooth film, which under the SEM is almost indistinguishable in appearance from the uncoated areas, although the border between coated and uncoated regions is clearly visible on the sample. No nanoparticles are observed anywhere in the coated region (Figure 15c). In contrast, nickel dewets the native tantalum oxide sur-

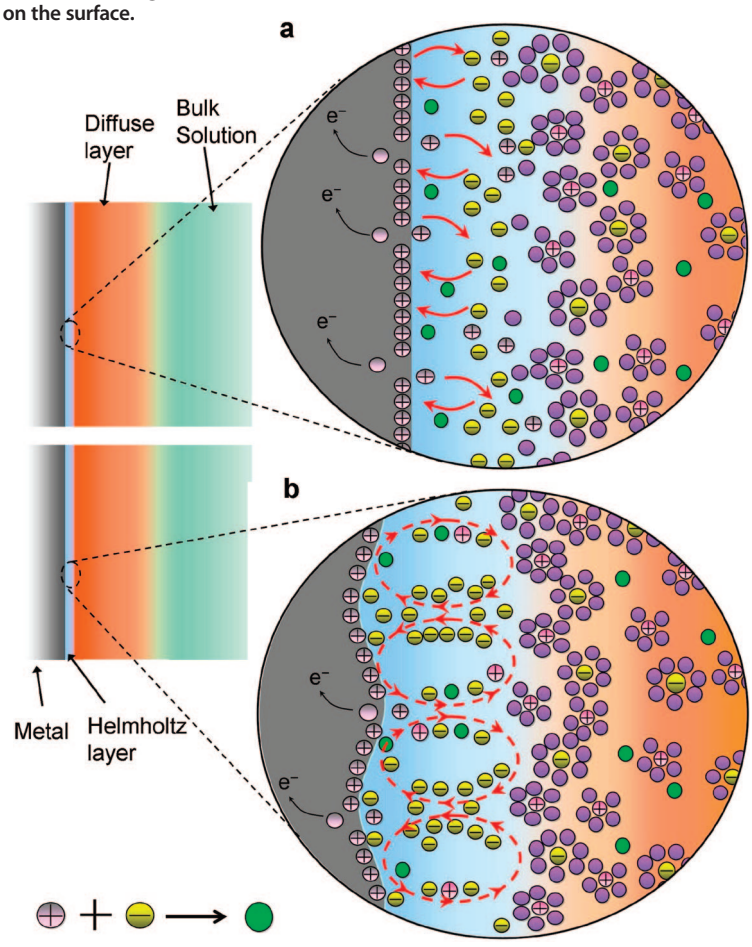

Figure 14. Mechanistic illustration of the Helmholtz layer under equilibrium and nonequilibrium conditions (not to scale) during the etching of the metal surface. (a) Undisturbed Helmholtz layer with minimal diffusion in the case of a very slow reaction. (b) Under vigorous reaction conditions, the layer may break up into convection cells to allow for fast electromigration of large amounts of reactants and products which leads to the dimpled morphology of the metal surface.

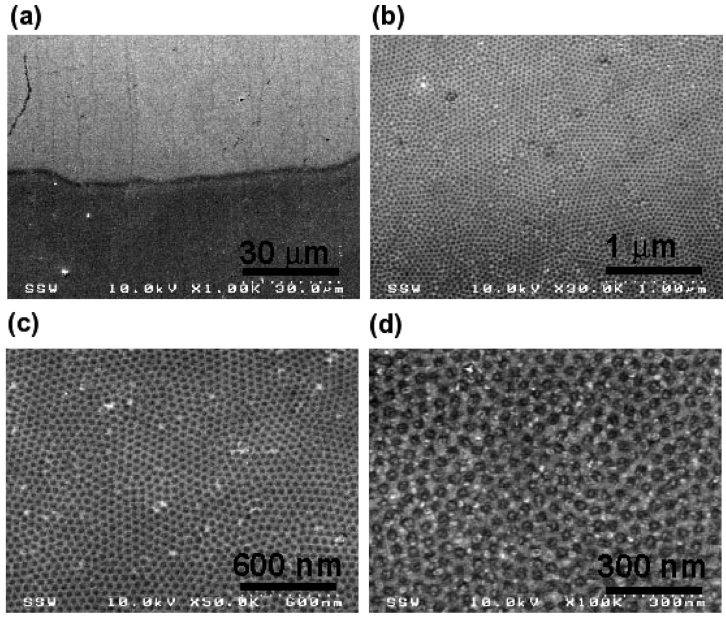

Figure 15. (a) Border between coated and uncoated regions of another dimpled tantalum sample with nominally 2 nm of Pt coated by e-beam evaporation after rapid thermal annealing to 650 °C; (b) close-up of border (coated region slightly darker at bottom); (c) coated region, showing a continuous film of Pt. (d) Coated and annealed region of another dimpled tantalum sample with nominally 2 nm of Ni coated by e-beam evaporation after rapid thermal annealing to 650 °C, showing Ni nanoparticles largely located in the pores.

face and forms nanoparticles that are evenly distributed inside the pores (Figure 15d). We have previously demonstrated dewetting with gold.[32] The nanoparticle formation is beneficial for catalytic purposes, but does not achieve the goal of large-scale dimple arrays of a particlar material. Materials such as nickel or gold can form metastable continuous films upon deposition, but they are subject to temperature limitations. Platinum, on the other hand, maintains the dimple morphology well. If the substrate was dissolved, it may be possible to fabricate an ultrathin platinum foil which would be mechanically reinforced by the dimple structure.

While our data does not give any insight into the initiation of the pattern formation process (less than 5 s from the start), other than the knowledge that it takes less than 0.5 s for the first dimples to appear (Figure 12b), the dominant process for the sustenance of the dimples appears to be electrohydrodynamic in nature.[40] The dimple formation is therefore analogous to Rayleigh−Benard convection[41] but effectively without boundary conditions since an electrode in our experiments is typically 5 mm wide and hence contains about 100 000 convection cells across. A similar model has previously been suggested for the case of electropolishing of steel.[42] It is tempting to suggest that it might apply to a variety of electropolishing systems under the right conditions, such as in the case of aluminum.[19]

CONCLUSION

Dimple formation has now been demonstrated with a high level of uniformity on tantalum, titanium, tungsten, and zirconium. Since the dimple structure is very robust, dimpled surfaces can be coated in thin films of other materials of interest, such as platinum, to further enhance the selection of dimpled materials. As we have demonstrated in this work, electrochemical dimple array formation is an astonishingly robust process. We are currently working on expanding it to other materials, such as titanium alloys for biomedical applications. In that context it will need to be considered that on chemically heterogeneous surfaces, pattern formation will occur selectively. A good example for that are nickel impurities on a tungsten surface, because nickel oxide is formed and not readily dissolved under the optimal conditions for dimple formation on tungsten. A perturbation in the dimple pattern can be observed near the nickel islands. Heterogeneous surface compositions will allow for area-selective pattern formation. The process is self-limiting and results in uniformly shallow features, which can then provide templates for subsequent processing[14] if higher aspect ratio features are desired for applications such as the formation of biocompatible surfaces for which the 50 nm length scale is very important[43] or as a template for catalyst nanoparticle formation.[32,44] Since the process is not tied to a specific chemistry, ordered dimple patterns can likely be formed on any conducting or semiconducting surface amenable to electropolishing, leading to a range of potential applications in sensor array fabrication,[45] combinatorial synthesis,[46] templated nanostructure growth, composite materials, electronics, catalysis, photovoltaics, and biomaterials.

METHODS

H_2SO_4 (95−98%, reagent grade), HF (48%), acetone, and methanol (both semiconductor grade) were purchased from Fisher Scientific. NH_4F (40%, semiconductor grade) was purchased from Sigma Aldrich. All chemicals were used as received. Tantalum (99.95%), titanium (99.95%), and zirconium foil (99.5%, all 0.127 mm thick) as well as tungsten ribbon (99.95%, 0.125 mm thick) and tungsten wire (d = 0.25 mm, 99.95%, all Alfa-Aesar) were mechanically cut and rinsed with acetone, methanol, and Millipore water (18.2 MΩ · cm resistivity) and then dried under argon flow before use. The Ta, Ti, W, and Zr surfaces were electropolished using a two-electrode system (Figure 1a) connected to an Agilent E3615A power supply. A Pt/Ir wire (0.25 mm diameter) was used as a cathode. Both electrodes were kept vertical, parallel to each other with an distance of approximately 1.5 cm. No attempt was made to moderate or control the temperature of the setup, even though the electropolishing reaction produced a significant amount of heat and the electrochemical cell warmed up well above room temperature. Ta, Ti, and W were

dimpled in a stirred mixture of concentrated H_2SO_4 (95−98%) and HF (48%) in volumetric ratios of 9:1 (Ta), 8:2 (Ti), and 93:7 (W) by applying a constant DC voltage of 15 V for 2 (Ti) and 10 min (W), respectively. Zr foil was dimpled in 0.5 M NH_4F at 20 V for 5 min. The typical sample size was 5 mm wide and 30 mm long, with one-third of the length immersed in the electrolyte. The solutions were stirred using a magnetic stir-bar. All samples were thoroughly rinsed with Millipore water (18.2 MΩ · cm resistivity) and then dried under argon flow after electropolishing. Freshly mixed electrolytic solutions typically needed to settle for 16−20 h before the first sample is processed.

For the metal deposition studies, several Ta samples were dimpled at 15 V for 10 min. Half of each sample was masked by spot-welding a piece of clean tantalum across the top, touching the dimpled surface; 2 nm each of nickel and platinum were separately electron-beam evaporated in a vacuum chamber at a rate of 0.1 nm/s onto several masked samples. The samples underwent rapid thermal annealing at 650 °C for 5 min in a nitrogen environment. E-beam evaporator and rapid thermal annealer are located in the Center for Emerging Device Technologies at McMaster University.

For the time-resolved studies, the electrodes were connected to a power supply (Kepco BOP 20−20 M) which was remote controlled by a LabVIEW program. The setup is capable of supplying a voltage pulse of variable time scales with a very short rise and decay time period (1 V/μs).

High-resolution TEM was carried out with a JEOL 2010 field emission TEM/STEM, operating at an accelerating voltage of 200 kV. The thin Ta section for cross-sectional analysis TEM was prepared by FIB milling at the Nanofab facility at the University of Western Ontario. The region of interest on the specimen was *in situ* coated with layers of carbon and platinum. The carbon layer gives a better contrast and the platinum layer protects the surface of the feature during subsequent FIB milling.

Atomic force microscopy was performed in tapping mode on a Veeco Enviroscope with a Nanoscope IIIa controller and Veeco RTESP n-doped Si tips with a nominal radius of less than 10 nm. Typical scan rates were 2 μm per second and the images were constructed with 512 scan lines. Care was taken to ensure that the tip was not modifying the surface during the scan. A large number of images of the same sample were obtained with different tips to pinpoint the exact depth of dimples by eliminating tip convolution effects. The data was analyzed using DI V5.30r3.sr3 software.

SEM imaging was performed with a JEOL JSM-7000F scanning electron microscope, equipped with a Schottky-type field emission gun (FEG) filament, except for the images in Figure 7 which were obtained on a Hitachi S-4500 FE-SEM. Energy dispersive X-ray (EDX) mapping was carried out using a 10 kV electron beam to obtain the distribution of O, Ni, and W on the electropolished W surface. INCA 300 (EDX System, Oxford, UK) software was used for data acquisition and analysis.

X-ray photoelectron spectra were measured using a Kratos Axis Ultra X-ray photoelectron spectrometer. XPS can detect all elements except hydrogen and helium, probes the surface of the sample to a depth of 7−10 nm, and has detection limits ranging from 0.1 to 0.5 atom % depending on the element. Survey scan analyses were carried out with an analysis area of 300 μm × 700 μm and pass energy of 160 eV. High resolution analyses were carried out with an analysis area of (300 × 700) micrometers and pass energy of 20 eV.

Acknowledgment. We are grateful to Todd Simpson (UWO) for preparing the TEM sample using FIB, Mark Biesinger (Surface Science Western) for providing the XPS analysis, Brian King (McMaster U.) for assistance with instrumentation, Ross Davidson (Surface Science Western) and Steve Koprich for help with SEM, and Fred Pearson and Christian Maunders (all Brockhouse Institute for Materials Research) for help with TEM. The work was financially supported by the Natural Science and Engineering Research Council of Canada and an Ontario Premier's Research Excellence Award.

Supporting Information Available: Additional SEM images and XPS spectra as well as certificates of analysis for metal substrates. This material is available free of charge *via* the Internet at http://pubs.acs.org.

REFERENCES AND NOTES

1. Stewart, M. E.; Motola, M. J.; Yao, J.; Thompson, L. B.; Nuzzo, R. G. Unconventional Methods for Forming Nanopatterns. *Proc. IMechE Part N* **2007**, *220*, 81–138.
2. Whitesides, G. M.; Grzbowski, B. Self Assembly at All Scales. *Science* **2002**, *295*, 2418–2421.
3. Stupp, S. I.; LeBohneur, V.; Walker, K.; Li, L. S.; Huggins, K. E.; Keser, M.; Amstutz, A. Supramolecular Materials: Self-Organized Nanostructures. *Science* **1997**, *276*, 384–389.
4. Henzie, J.; Barton, J. E.; Stender, C. L.; Odom, T. W. Large-Area Nanoscale Patterning: Chemistry Meets Fabrication. *Acc. Chem. Res.* **2006**, *39*, 249–257.
5. Pawin, G.; Wong, K. L.; Kwon, K. Y.; Bartels, L. A Homomolecular Porous Network at a Cu(111) Surface. *Science* **2006**, *313*, 961–962.
6. Qiao, Y.; Wang, D.; Buriak, J. M. Block Copolymer Templated Etching on Silicon. *Nano Lett.* **2007**, *7*, 464–469.
7. Bullen, H. A.; Garrett, S. J. TiO_2 Nanoparticle Arrays Prepared Using a Nanosphere Lithography Technique. *Nano Lett.* **2002**, *2*, 739–745.
8. Landolt, D.; Chauvy, P.-F.; Zinger, O. Electrochemical Micromachining, Polishing and Surface Structuring of Metals: Fundamental Aspects and New Developments. *Electrochim. Acta* **2003**, *48*, 3185–3201.
9. Thompson, G. E.; Furneaux, R. C.; Wood, G. C.; Richardson, J. A.; Goode, J. S. Nucleation and Growth of Porous Anodic Films on Aluminum. *Nature* **1978**, *272*, 433–435.
10. Masuda, H.; Fukuda, K. Ordered Metal Nanohole Arrays Made by a 2-Step Replication of Honeycomb Structures of Anodic Alumina. *Science* **1995**, *268*, 1466–1468.
11. Lee, W.; Ji, R.; Gosele, U.; Nielsch, K. Fast Fabrication of Long-Range Ordered Porous Alumina Membranes by Hard Anodization. *Nat. Mater.* **2006**, *5*, 741–747.
12. Cai, Q. Y.; Paulose, M.; Varghese, O. K.; Grimes, C. A. The Effect of Electrolyte Composition on the Fabrication of Self-Organized Titanium Oxide Nanotube Arrays by Anodic Oxidation. *J. Mater. Res.* **2005**, *20*, 230–236.
13. Sieber, I.; Kannan, B.; Schmuki, P. Self-Assembled Porous Tantalum Oxide Prepared in H_2SO_4/HF Electrolytes. *Electrochem. Solid State Lett.* **2005**, *8*, J10–J12.
14. Singh, S.; Greiner, M. T.; Kruse, P. Robust Inorganic Membranes from Detachable Ultra-Thin Tantalum Oxide Films. *Nano Lett.* **2007**, *7*, 2676–2683.
15. Sieber, I.; Hildebrand, H.; Friedrich, A.; Schmuki, P. Formation of Self-Organized Niobium Porous Oxide on Niobium. *Electrochem. Commun.* **2005**, *7*, 97–100.
16. Jessensky, O.; Muller, F.; Gosele, U. Self-Organized Formation of Hexagonal Pore Arrays in Anodic Alumina. *Appl. Phys. Lett.* **1998**, *72*, 1173–1175.
17. Bandyopadhyay, S.; Miller, A. E.; Chang, H. C.; Banerjee, G.; Yuzhakov, V.; Yue, D.-F.; Ricker, R. E.; Jones, S.; Eastman, J. A.; Baugher, E.; Chandrasekhar, M. Electrochemically Assembled Quasi-Periodic Quantum Dot Arrays. *Nanotechnology* **1996**, *7*, 360–371.
18. Konovalov, V. V.; Zangari, G.; Metzger, R. M. Highly Ordered Nanotopographies on Electropolished Aluminum Single Crystals. *Chem. Mater.* **1999**, *11*, 1949–1951.
19. Caicedo-Martinez, C. E.; Koroleva, E. V.; Thompson, G. E.; Skeldon, P.; Shimizu, K.; Habazaki, H.; Hoellrig, G. *Surf. Nanotextures Al Surf. Interface Anal.* **2002**, *34*, 405–408.
20. Koroleva, E. V.; Thompson, G. E.; Skeldon, P.; Noble, B. Crystallographic Dissolution of High Purity Aluminium. *Proc. R. Soc., A* **2007**, *463*, 1729–1748.
21. Zhao, G.-Y.; Xu, C.-L.; Guo, D.-J.; Li, H.; Li, H.-L. Patterning Polycrystalline Aluminum by Electropolishing at Low Voltages. *J. Solid State Electrochem.* **2006**, *10*, 266–269.
22. Yuzhakov, V. V.; Chang, H.-C.; Miller, A. E. Pattern Formation during Electropolishing. *Phys. Rev. B* **1997**, *56*, 12608.

23. Yuzhakov, V. V.; Takhistov, P. V.; Miller, A. E.; Chang, H. C. Pattern Selection during Electropolishing due to Double-Layer Effects. *Chaos* **1999**, *9*, 62–77.
24. Guo, W. D.; Johnson, D. T. Pattern Selection with Anisotropy during Aluminum Electropolishing. *J. Cryst. Growth* **2004**, *268*, 258–271.
25. Guo, W. D.; Johnson, D. T. Role of Interfacial Energy during Pattern Formation of Electropolishing. *Phys. Rev. B* **2003**, *67*, 075411.
26. Tappin, D. K.; Robertson, I. M.; Birnbaum, H. K. On the Formation of a Periodic Surface Structure on Zr_3Al during Anodic Dissolution. *Acta Mater.* **1996**, *44*, 135–146.
27. Krasteva, I.; Koper, M. T. M. Pattern Formation during the Electrodeposition of a Silver-Antimony Alloy. *Phys. A* **1995**, *213*, 199–208.
28. Andryushchenko, T. N.; Miller, A. E.; Fischer, P. B. Long Wavelength Roughness Optimization during Thin Cu Film Electropolish. *Electrochem. Solid State Lett.* **2006**, *9*, C181–C184.
29. Cathcart, J. V.; Bakish, R.; Norton, D. R. Oxidation Properties of Tantalum Between 400° and 530°C. *J. Electrochem. Soc.* **1960**, *107*, 668–670.
30. Pawel, R. E.; Lundy, T. S. A Submicron Sectioning Technique for Analyzing Diffusion Specimens of Tantalum and Niobium. *J. Appl. Phys.* **1964**, *35*, 435–438.
31. Ueno, K.; Abe, S.; Onoki, R.; Saiki, K. Anodization of Electrolytically Polished Ta Surfaces for Enhancement of Carrier Injection into Organic Field-Effect Transistors. *J. Appl. Phys.* **2005**, *98*, 114503.
32. El-Sayed, H.; Singh, S.; Greiner, M. T.; Kruse, P. Formation of Highly Ordered Arrays of Dimples on Tantalum at the Nanoscale. *Nano Lett.* **2006**, *6*, 2995–2999.
33. El-Sayed, H.; Singh, S.; Kruse, P. Formation of Dimpled Tantalum Surfaces from Electropolishing. *J. Electrochem. Soc.* **2007**, *154*, C728–C732.
34. Vermilyea, D. A. Formation of Anodic Oxide Films on Tantalum in Non-Aqueous Solutions. *Acta Metall.* **1954**, *2*, 483–486.
35. Krischer, K.; Mazouz, N.; Grauel, P. Fronts, Waves and Stationary Patterns in Electrochemical Systems. *Angew. Chem., Int. Ed.* **2001**, *40*, 850–869.
36. Mazouz, N.; Krischer, K. A Theoretical Study on Turing Patterns in Electrochemical Systems. *J. Phys. Chem. B* **2000**, *104*, 6081–6090.
37. Krischer, K. New Directions and Challenges in Electrochemistry—Spontaneous Formation of Spatiotemporal Patterns at the Electrode−Electrolyte Interface. *J. Electroanal. Chem.* **2001**, *501*, 1–21.
38. Pritzker, M. D.; Fahidy, T. Z. Morphological Stability of a Planar Metal Electrode during Potentiostatic Electrodeposition and Electrodissolution. *Electrochim. Acta* **1992**, *37*, 103–112.
39. Lehmann, V. *Electrochemistry of Silicon: Science, Materials and Applications*; Wiley-VCH: Weinberg, Germany, 2002.
40. Van Tassel, J. J.; Randall, C. A. Ionic Gradients at an Electrode above the Equilibrium Limit Current. 2. Transition to Convection. *J. Phys. Chem. C* **2007**, *111*, 3349–3357.
41. Cross, M. C.; Hohenberg, P. C. Pattern Formation Outside of Equilibrium. *Rev. Mod. Phys.* **1993**, *65*, 851–1112.
42. Vignal, V.; Roux, J. C.; Flandrois, S.; Fevrier, A. Nanoscopic Studies of Stainless Steel Electropolishing. *Corros. Sci.* **2000**, *42*, 1041–1053.
43. Cavalcanti-Adam, E. A.; Volberg, T.; Micoulet, A.; Kessler, H.; Geiger, B.; Spatz, J. Cell Spreading and Focal Adhesion Dynamics are Regulated by Spacing of Integrin Ligands. *Biophys. J.* **2007**, *92*, 2964–2974.
44. Wu, Z. H.; Mei, X. Y.; Kim, D.; Blumin, M.; Ruda, H. E. Growth of Au-Catalyzed Ordered GaAs Nanowire Arrays by Molecular-Beam Epitaxy. *Appl. Phys. Lett.* **2002**, *81*, 5177–5179.
45. Furhop, J.-H. Molecular Interactions in Solvent-Filled Yoctowells (10^{-24} L) and Zeptowells (10^{-21} L). *Curr. Opin. Colloid Interface Sci.* **2008**, *13*, 81–85.
46. Barton, J. E.; Odom, T. W. Mass-Limited Growth in Zeptoliter Beakers: A General Approach for the Synthesis of Nanocrystals. *Nano Lett.* **2004**, *4*, 1525–1528.